



## Co-aromatization of methane with olefins: The role of inner pore and external surface catalytic sites



Peng He<sup>a</sup>, Jack Jarvis<sup>a</sup>, Shijun Meng<sup>a</sup>, Aiguo Wang<sup>a</sup>, Shiyu Kou<sup>a</sup>, Richard Gatip<sup>a</sup>, Matthew Yung<sup>b</sup>, Lijia Liu<sup>c</sup>, Hua Song<sup>a,\*</sup>

<sup>a</sup> Department of Chemical and Petroleum Engineering, University of Calgary, 2500 University Drive NW, Calgary, Alberta, T2N 1N4, Canada

<sup>b</sup> National Bioenergy Center, National Renewable Energy Laboratory, 15013 Denver West Parkway, Golden, CO, 80401, United States

<sup>c</sup> Jiangsu Key Laboratory for Carbon-Based Functional Materials & Devices, Institute of Functional Nano and Soft Materials (FUNSOM), Soochow University-Western University Centre for Synchrotron Radiation Research, Soochow University, Suzhou, Jiangsu, 215123, China

### ARTICLE INFO

#### Keywords:

Methane co-aromatization  
Pore size  
Selectivity  
Isotope labelling  
Post-synthetic treatment

### ABSTRACT

The co-aromatization of methane with olefins is investigated using Ag-Ga/HZSM-5 as the catalyst at 400 °C. The presence of methane has a pronounced effect on the product distribution in terms of increased average carbon number and substitution index and decreased aromatic carbon fraction compared with its N<sub>2</sub> environment counterpart. The participation of methane during the co-aromatization over the Ag-Ga/HZSM-5 catalyst diminishes as the co-fed olefin feedstock molecule becomes larger, from 1-hexene to 1-octene and 1-decene, in diameter. The effect of suppressed methane participation with larger olefinic molecules is not as significant when Ag-Ga/HY is employed as the catalyst, which might be attributed to the larger pore size of HY that gives more room to hold olefin and methane molecules within the inner pores and reduces the diffusion limitation of olefin molecules. The effect of olefin feedstock on the methane participation during the co-aromatization over Ag-Ga/HZSM-5 is experimentally evidenced by <sup>13</sup>C and <sup>2</sup>D NMR. The incorporation of the methane carbon atoms into the phenyl ring of product molecules is reduced significantly with larger co-fed olefins, whereas its incorporation into the substitution groups of the formed aromatic molecules is not notably affected, suggesting that the methane participation in the phenyl ring formation might preferably occur within inner pores, while its incorporation into substitution groups may mainly take place on external catalytic sites. This hypothesis is well supported by the product selectivity obtained over Ag-Ga/HZSM-5 catalysts prepared using conventional ZSM-5, ZSM-5 with the external catalytic sites deactivated, nanosize ZSM-5, ZSM-5 with a micro/meso pore structure and ZSM-5 with the inner pores blocked, and further confirmed by the isotopic labeling studies.

### 1. Introduction

Catalytic transformation of methane, the major component of natural gas, into more valuable carbon-containing products has provided an effective alternative for the use of natural gas. However, the inert structure of methane prohibits its conversion into more value-added chemicals and fuels. Methane must follow multistep conversion strategies via syngas and/or methanol before it can be transformed into higher hydrocarbons, resulting in increased costs and impeding its commercial potential. In 2017, the price of Henry Hub natural gas averaged US \$3.10 per million British thermal units (MBTU), while that of the West Texas Intermediate (WTI) light sweet crude oil averaged at US \$50.8 per barrel, which equates to US \$9.15 per MBTU. The greatly underutilized value of methane has driven researchers to investigate methods that can potentially boost the profitability of the natural gas

industry, the necessity of this goal is highlighted given current era of low energy prices. The conversion of low cost methane into high value commodities including more commercially useful chemicals and liquid fuels has attracted special attentions. However, due to its symmetric molecular structure, methane activation presents a great challenge for the entire catalysis field. Oxidative coupling of methane to convert it into more valuable chemicals such as ethylene and methanol has been extensively studied [1–4]. An increased methane conversion, however, often comes with a loss in selectivity due to the production of CO and CO<sub>2</sub> as well as the more prominent reactivity of desired products compared with methane, resulting in significantly reduced desirable product yield. On the other hand, the direct transformation of methane into liquid chemicals such as aromatics has also been explored under non-oxidative environment over the last few decades [5–13]. The commercialization of this process, however, is impeded by the low

\* Corresponding author.

E-mail address: [sonh@ucalgary.ca](mailto:sonh@ucalgary.ca) (H. Song).

product yield and high reaction temperature, which are often above 700 °C. Nevertheless, the conversion of methane at lower temperatures (400–600 °C) is significantly enhanced when co-fed with hydrocarbons [14–25]. In the co-aromatization process of methane and propylene, the participation of methane into the products is verified by a series of techniques including isotopic labelling [26]. It is noticed that both the metal species and the –OH groups of the zeolite framework, which act as strong Bronsted acid sites, catalyze the methane activation and conversion process [20,27,28]. The reaction between methane and –OH groups of Ag-Ga/HZSM-5 catalysts was evidenced by deuterium isotopic labelling [26]. Wang et al. [29] observed that the metal modification of HZSM-5 by Ag and Ga would enhance the methane conversion. A rational catalyst design to achieve improved methane participation and desired product selectivity, however, requires a comprehensive understanding of the co-aromatization mechanism. A more accurate picture of the methane participation pathways thus must be obtained. Over the zeolite based catalysts, the zeolite topology often imposes a pronounced effect on the reaction pathways [30–36] due to the effect of topology on the diffusion of guest molecules, accessibility to catalytic sites and tolerance to coke formation. Hydrogen transfer is a crucial step in the conversion of hydrocarbons and the aromatization process, with large spatial requirements needed to facilitate this bimolecular process. Lukyanov et al. [37] observed that aromatization capacities of TON-type zeolite and HZSM-5, despite their similar pore size, are different, and attributed this phenomenon to the channel intersection in HZSM-5 that facilitates the bimolecular hydrogen transfer step. Thus, the modification of Ga, which acts as a dehydrogenating center and lessens the dependence on the hydrogen transfer step during aromatization, witnesses a more profound aromatization improvement on TON. Besides reactivity, the channel interconnections of ZSM-5 also impose a notable influence on the product selectivity compared with straight channel zeolites [38]. Teketel et al. [39] observed that the confinement effect of zeolite cavities had a significant influence on the methylation and C–H cleavage steps of the hydrocarbon intermediates in the zeolite cages [40]. The conversion of naphtha oil and 1-octene to diesel components has been studied over ITQ-39 zeolite catalyst, where the alkylation reaction take place on the external acid sites ascribed to the restriction of the zeolite structure [41].

Previous research has suggested that the co-aromatization of methane and other hydrocarbon molecules prefers to occur within the inner pores of zeolite based catalysts [21]. Kosinov et al. [42] studied the conversion of CH<sub>4</sub> to benzene over Mo/HZSM-5 at 700 °C and attributed the aromatization capacity to the MoC<sub>x</sub> species dispersed in the micropores of ZSM-5. However, getting a comprehensive understanding on the function of the sites located on the inner and external pores is challenging. Ding et al. [43] investigated the effect of silanation of external acid sites on the product selectivity during CH<sub>4</sub> aromatization over Mo/HZSM-5. It was observed that the selectivity of large aromatic molecules is decreased if the preferred catalytic sites are located in the inner pores, where the bimolecular reaction and transition states formation are suppressed by the spatial constraints. Recently, some researchers explored the feasibility of selectivity control by introducing organic molecules that have non-covalent interactions with specific active sites [44,45], which presents an effective approach to identify the function of specific catalytic active sites. Large organic compounds that cannot diffuse into the inner pores of ZSM-5, such as 3-amino-propyl-triethoxysilane, are employed to cover the external acid sites. Recently, Kim et al. [46] prepared zeolites with the inner pores covered by carbon deposits while external sites free of coke deposit through La- or Ca-exchange followed by ethylene treatment at 600 °C. It was observed that the coke formation on Ca-ZSM-5 is favorable within the inner pores, resulting in carbon particles with identical shapes and diameters of the inner pores. This approach can be employed to selectively deactivate catalytic sites within the inner pores by blocking the inner pores themselves and thus, aid with probing the function of these sites. Besides deactivation of the inner pore sites, their catalytic activity

and product selectivity can be influenced by the introduction of mesopores in the hierarchical zeolite structure [47–51], which bring additional external surface area.

This paper thus systematically studies the effect of various catalytic sites on the co-aromatization of methane and olefins in terms of product selectivity, methane participation and feedstock conversion at a low temperature of 400 °C by employing the aforementioned selective surface deactivation and/or modification strategies. The co-aromatization of methane with various co-fed olefin feedstocks over Ag-Ga/HZSM-5 and Ag-Ga/HY are carried out to study the effect of feedstock size and catalyst pore size. The methane participation in the co-aromatization reaction with different co-fed olefins is demonstrated directly using the <sup>13</sup>C and <sup>2</sup>D isotope labelling method. Four kinds of HZSM-5 support materials including HZSM-5 with surface acid sites covered by SiO<sub>2</sub>, conventional HZSM-5, HZSM-5 with micro/meso pore hierarchical structure and HZSM-5 with its inner pores blocked by coke deposits, are employed to manipulate the ratio of catalytic sites located in the inner pore and on the external pore surface.

## 2. Experimental

### 2.1. Synthesis of catalysts

Ammonium type ZSM-5 (NH<sub>4</sub>-ZSM-5) and hydrogen type Zeolite Y (HY) with a SiO<sub>2</sub>/Al<sub>2</sub>O<sub>3</sub> ratio of 80:1 were obtained from Zeolyst USA. NH<sub>4</sub>-ZSM-5 was converted into H-ZSM-5 by calcination at 600 °C in ambient air for 3 h. The metal-modified HZSM-5 was prepared by wetness impregnation method. 0.13 g AgNO<sub>3</sub> (Sigma Aldrich, 99.9+%) and 0.30 g Ga(NO<sub>3</sub>)<sub>3</sub>·xH<sub>2</sub>O (99.9%, Alfa Aesar) were dissolved in 10 g deionized (DI) water to form the aqueous solution of the metal precursors, which was then impregnated into H-ZSM-5 for preparing 1 wt. %Ag-1 wt.%Ga/ZSM-5. The obtained wet powder was dried in the oven at 92 °C overnight, followed by calcination at 600 °C for 3 h in ambient air. The reason for choosing the combination of Ag and Ga over using solely Ag and Ga is based on the authors' previous work on olefin reduction in heavy oil cracking distillates [25]. Comparing with that when solely Ag or Ga is engaged, a larger olefin conversion is witnessed when both of them are introduced to the catalyst. The Ag and Ga species tend to form partially reduced mixed metal oxides after the reaction under methane environment, while larger particles are formed under N<sub>2</sub> environment. This phenomenon suggest that there may be some interaction between Ag, Ga and methane in the reaction with olefins, which might facilitate methane conversion. A similar phenomenon is observed in the co-aromatization reactions between methane and propylene, where the modification of HZSM-5 using Ag and Ga enhances methane participation [26].

ZSM-5 support with external acid sites covered by SiO<sub>2</sub> was prepared following the procedure described in reference [43]. Ag-Ga/HZSM-5 sample was immersed in ethanol containing 3-aminopropyl-triethoxysilane (Aldrich, 99%) and stirred for 2 h. Ethanol was evaporated at 80 °C. The sample was then dried at 110 °C and calcined at 550 °C for 4 h.

Nanosize ZSM-5 was prepared following the procedure described in reference [52]. First, S-1 gel was prepared to use as seeds. 10.98 g of TEOS, used as silica source, was added dropwise into 10.5 g 1.0 M TPAOH (Sigma Aldrich) solution mixed with 15 mL deionized water and 10.0 g EtOH while stirring. After stirring at room temperature for 2 h, the mixture was transferred to a Teflon-lined autoclave and kept at 100 °C for 96 h. 0.69 g NaOH, 0.17 g NaAlO<sub>2</sub> and 0.66 g Hexadecyltrimethylammonium bromide (99%, Sigma Aldrich) were dissolved in 30 g H<sub>2</sub>O. After stirring for 0.5 h, 6.5 g S-1 gel and 12.5 g silica sol were dropwise added into the clear solution in sequence under agitation. The mixture was stirred at ambient temperature for 2 h, and transferred into a Teflon-lined autoclave. The autoclave was kept at 120 °C for 12 h before ramped to and kept at 170 °C for 24 h. The products were centrifuged and washed with H<sub>2</sub>O until the pH reached about 8. The

recovered powder was dried at 110 °C for 5 h, and calcined at 550 °C for 6 h to obtain nanosize Na-ZSM-5. Ion exchange with 0.5 mol/L NH<sub>4</sub>NO<sub>3</sub> aqueous solution was carried out in triplicate at 80 °C, followed by calcination at 550 °C for 2 h. 1 wt.% Ag and 1 wt.% Ga was loaded onto the obtained nanosize HZSM-5 using the aforementioned approach.

ZSM-5 support with micro/meso hierarchical structure was prepared following the procedure described in reference [53]. NH<sub>4</sub>-ZSM-5 was treated by 0.2 mol/L NaOH aqueous solution at 65 °C for 30 min and quenched in an ice-water mixture. The sample was recovered by centrifuge and washed with DI H<sub>2</sub>O. Ion exchange with 0.5 mol/L NH<sub>4</sub>NO<sub>3</sub> aqueous solution was carried out in triplicate at 80 °C, followed by calcination at 550 °C for 2 h. 1 wt.% Ag and 1 wt.% Ga was loaded onto the obtained micro/meso hierarchical HZSM-5 using the aforementioned approach.

ZSM-5 support with its inner pores blocked was prepared following the procedure describe in reference [46]. Ion-exchange of NH<sub>4</sub>-ZSM-5 with 0.1 mol/L Ca(NO<sub>3</sub>)<sub>2</sub> aqueous solution (prepared with Ca (NO<sub>3</sub>)<sub>2</sub>·4H<sub>2</sub>O, Alfa Aesar, 99%) at 80 °C was conducted in triplicate, followed by calcination at 550 °C for 2 h. The obtained Ca-ZSM-5 sample was loaded to a lab fabricated flow reactor and kept at 600 °C under N<sub>2</sub> flow for 2 h and a mixture of ethylene and N<sub>2</sub> for another 1 h. The sample was then collected and ion-exchanged with 0.5 mol/L NH<sub>4</sub>NO<sub>3</sub> aqueous solution at 80 °C for 3 times to convert any remaining active Ca sites into ammonium sites. 1 wt.% Ag and 1 wt.% Ga was then loaded to the resulting support material using the aforementioned approach.

## 2.2. Catalytic performance evaluation

The olefin upgrading reactions were carried out in a 100 mL batch reactor manufactured by Parr Instrument and is capable of tolerating high temperatures up to 500 °C and high pressures up to 35 MPa. The diameter and length of the reactor cylinder are 5 cm and 12 cm, respectively. In a typical run, 0.1 g catalyst and a glass vial carrying 0.1 g olefin feedstock, such as 1-hexene (98%, Alfa Aesar), 1-octene (98%, Alfa Aesar) and 1-decene (96%, Alfa Aesar), were put at the bottom of the reactor cylinder. These feedstocks were put into the vial so that they would contact the catalyst with the catalyst as gas components along with the methane molecules in the gas phase when heated up. The reactor was purged and pressurized to 5.0 MPa with methane (99.97%, Praxair). When ethylene (99.5%, Praxair) and 1-butene (99.5% Praxair) were employed as the feedstock, the reactor was purged and then pressurized to 0.05 MPa by ethylene or 1-butene (partial pressure of 0.15 MPa), followed by the introduction of methane to a total pressure of 5.0 MPa. N<sub>2</sub> (99.998%, Praxair) was also used to pressurize the reactor in control group reactions. The reactor temperature was then ramped up with a rate of 20 °C/min to the destination temperature (400 °C) and held for 60 min. The reactor was sealed during the reaction and the pressure would be increased to 9.0–9.5 MPa. Upon reaction completion, the reactor was allowed to cool down to room temperature before product collection. The gas product was discharged to a 2.2 L cylinder, which was previously purged by N<sub>2</sub>. The temperature and pressure (0.25–0.35 MPa) were recorded before the gas product was analyzed by micro-GC. The formed liquid product embedded into the charged solid catalyst was extracted out using 10.0 g CS<sub>2</sub> (GC grade, EMD Chemicals) as solvent and internal standard for following nuclear magnetic resonance spectroscopy (NMR) analysis in each batch of reaction.

Reaction between olefin feedstocks and <sup>13</sup>CH<sub>4</sub> and CD<sub>4</sub> (99.9% <sup>13</sup>C and 99% <sup>2</sup>D, respectively, Cambridge Isotope Laboratories, Inc.) were conducted in a similar manner when 0.5 g catalyst was charged. The reactor was pressurized to 0.3 MPa by <sup>13</sup>CH<sub>4</sub> or CD<sub>4</sub> after the reactor was purged by N<sub>2</sub>.

The composition of the product oil was determined by the pre-calibrated Gas Chromatography-Mass Spectrometer (GC-MS: PerkinElmer GC Claus 680 and MS Clarus SQ 8 T) equipped with a Paraffins-Olefins-

Naphthenes-Aromatics (PONA) column (Agilent HP-PONA). The oven temperature of the GC was programmed to hold at 35 °C for 15 min, ramp to 70 °C at 1.5 °C/min, rise to 150 °C at 3 °C/min and hold for 30 min, then ramp to 250 °C at 3 °C/min and hold for 2 min.

The gas products were analyzed by an on-line four-channel micro-GC (490, Agilent) equipped with thermal conductivity detectors, which can precisely analyze H<sub>2</sub>, O<sub>2</sub>, N<sub>2</sub>, CH<sub>4</sub>, and CO in the first channel equipped with a 10 m molecular sieve 5 A column; CO<sub>2</sub>, C<sub>2</sub>H<sub>2</sub>, C<sub>2</sub>H<sub>4</sub>, and C<sub>2</sub>H<sub>6</sub> in the second channel installed with a 10 m PPU column; and C<sub>3</sub>–C<sub>6</sub> and C<sub>3</sub>=–C<sub>5</sub>= in the third and fourth channels charged with a 10 m alumina column and a 8 m CP-Sil 5 CB column, respectively. Ar and He are the carrier gases for the first and remaining three channels, respectively. The composition of the gas products were used to calculate the moles of each species.

The average carbon number of product molecules is calculated based on the molar fraction of product molecules with variable carbon numbers. The molar fraction (*y<sub>i</sub>*) of each molecule with formula C<sub>x</sub>H<sub>*i*</sub> in the molecule matrix is obtained by GC-MS analysis of the products. The average carbon number is calculated by

$$\text{Average Carbon Number} = \sum (x_i \times y_i)$$

The substitution index demonstrates the fraction of carbon atoms that are attached to substitute groups among the phenyl ring carbon atoms in the product molecules matrix. The molar fraction (*y<sub>i</sub>*) of each molecule, which has *m* carbon atoms on the phenyl rings along with *n* substitution groups, is obtained by GC-MS analysis of the products. The substitution index is calculated by

$$\text{Substitution Index} = \sum \left( \frac{n_i}{m_i} \times y_i \right)$$

The aromatic carbon fraction is the fraction of carbon atoms on the phenyl rings among all the carbon atoms in the product matrix. The molar fraction (*y<sub>i</sub>*) of each molecule, which has *m* carbon atoms on the phenyl rings and *n* carbon atoms on the substitution groups, is obtained by GC-MS analysis of the products. The aromatic carbon fraction is calculated by

$$\text{Aromatic carbon fraction} = \sum \left( \frac{m_i}{m_i + n_i} \times y_i \right)$$

The error values of average carbon number, substitution index and aromatic carbon fraction in the present work are determined to be 0.02, 0.002 and 0.002, respectively.

## 2.3. Sample characterizations

The <sup>1</sup>H NMR experiments were conducted at 9.4 T (*v<sub>0</sub>*(<sup>1</sup>H) = 400.1 MHz) on a BRUKER AVANCEIII 400 spectrometer with a BBFO probe. <sup>1</sup>H NMR chemical shifts were referenced to CHCl<sub>3</sub> at 7.28 ppm. A spectral width of 12 kHz and a pulse delay of 3.5 s were used to acquire 64 scans per spectrum. The NMR samples in the tubes were prepared by mixing 0.30 mL sample with 0.30 mL CDCl<sub>3</sub> (99.8% atom D, Sigma). The trace amount of CHCl<sub>3</sub> in CDCl<sub>3</sub> functions as an internal standard.

The <sup>2</sup>D NMR experiments were conducted at 9.4 T (*v<sub>0</sub>*(<sup>2</sup>D) = 61.4 MHz) on a BRUKER AVANCEIII 400 spectrometer with a BBFO probe. A spectral width of 2.5 kHz and a recycle delay of 7 s were used to acquire 512 scans per spectrum.

The <sup>13</sup>C NMR experiments were conducted at 14.1 T (*v<sub>0</sub>*(<sup>13</sup>C) = 150.9 MHz) on a BRUKER AVANCEIII 600 spectrometer using a zgpg30 pulse program. <sup>13</sup>C NMR chemical shifts were referenced to CDCl<sub>3</sub> at 77.23 ppm. A spectral width of 36 kHz and a recycle delay of 2 s were used to acquire 10,000 scans per spectrum. The NMR samples in the tubes were prepared by mixing 0.50 mL sample with 0.10 mL CDCl<sub>3</sub>.

STXM measurements were conducted at the SM beamline (10ID-1) at the Canadian Light Source (CLS), which is equipped with a 35 nm

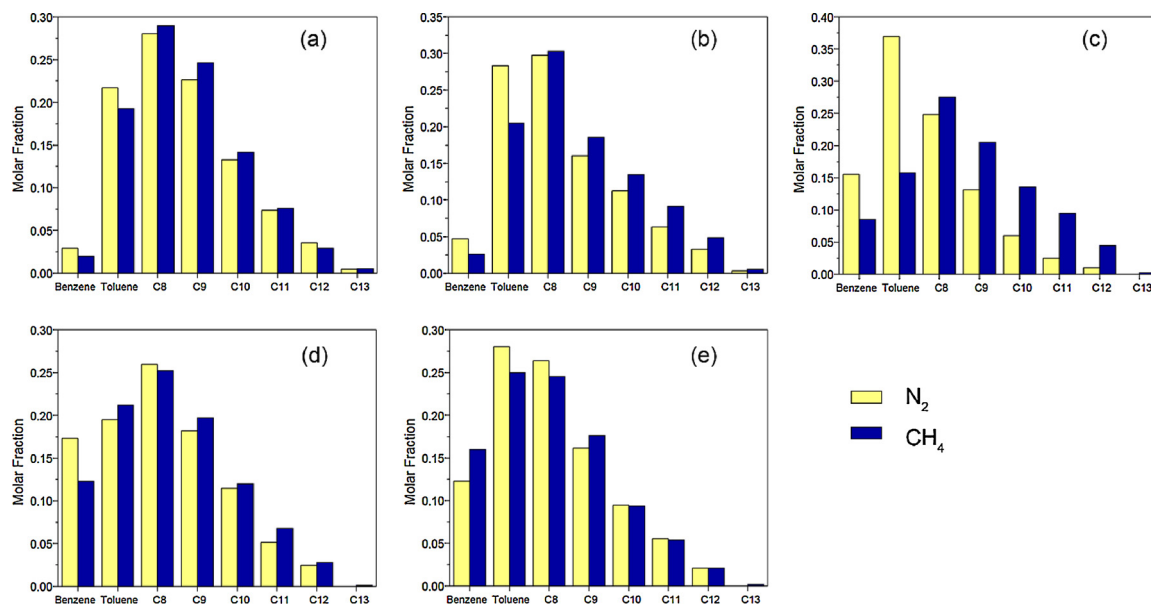


**Fig. 1.** The component distribution of the liquid products obtained from the reaction between (a) ethylene (b) 1-butene (c) 1-hexene (d) 1-octene and (e) 1-decene with methane over Ag-Ga/HZSM-5 at 400 °C and 5.0 MPa.

outermost-zone plate (CXRO, Berkeley Lab). The procedure is similar to that described in reference [54]. The diffraction-limited spatial resolution for this zone plate is 30 nm. Image sequence (stack) scans over a range of photon energies were acquired for the same sample region at the Zn L<sub>3,2</sub>-edge. The STXM data was analyzed using the aXis2000 software package. More details of the sample preparation and STXM measurements are included in the Supporting Information.

Determination of the quantities of chemical elements present in each sample by inductively coupled plasma atomic emission spectroscopy (ICP-AES) was performed using a Shimadzu ICPE-9000 multi-type emission spectrometer using Ar (99.999%, Praxair) as the plasma gas, the auxiliary gas and the carrier gas. Prior to measurement, a 90 s solvent rinse followed by a 90 s sample rinse were run. Each sample was then measured for 30 s three times in a row. Zeolite samples was dissolved in nitric acid and diluted by ultrapure water before the ICP measurement. The blank test sample was prepared in exactly the same way using ultrapure water without sample addition. The weight percentages of Ag and Ga of Ag-Ga/HZSM-5 are determined to be 0.62% and 0.37%, respectively. The weight percentages of Ag and Ga of Ag-Ga/HY are determined to be 0.66% and 0.40%, respectively.

#### 2.4. Theoretical calculation

The geometry structure of 3-aminopropyl-triethoxysilane (3AT) molecule was optimized by using Dmol3 module in Material studio. The calculation of molecular diameter follows the following equation:

$$d = d_{12} + r_1 + r_2$$

In this equation,  $d_{12}$  is distance between two furthest atoms. The Van der Waals radius values of these two atoms also contributed to the molecular diameter, which were represented by  $r_1$  and  $r_2$ . The Van der Waals radius of hydrogen atom was 1.2 Å.

The molecular energy and adsorption energy calculations were also conducted in Material Studio using Dmol3 module. The energy of 3-aminopropyl-triethoxysilane and one-cell ZSM-5 were calculated as  $E_{3AT}$  and  $E_{ZSM5}$ , respectively. The adsorption energy of the system ( $E_{ad}$ ) with 3-aminopropyl-triethoxysilane molecule in the ZSM-5 framework was also calculated by following equation:

$$E_{ad} = E_{3AT/ZSM5} - E_{3AT} - E_{ZSM5}$$

### 3. Results and discussions

#### 3.1. Methane co-aromatization with olefins over Ag-Ga/HZSM-5

The products obtained from the reaction of ethylene, 1-butene, 1-hexene, 1-octene and 1-decene under 5.0 MPa  $N_2/CH_4$  when Ag-Ga/HZSM-5 is employed as the catalyst are analyzed and determined to be composed of aromatics such as benzene, toluene and C<sub>8</sub>–C<sub>13</sub> aromatics, while olefin feedstocks are not detected in the liquid products. Ethylbenzene and xylenes are the products observed in the C<sub>8</sub> group, among which *p*-xylene and *o*-xylene are the major components. C<sub>9</sub>–C<sub>13</sub> products include the species with methyl, ethyl, propyl, groups, or their combinations attached to benzene and naphthalene as substituent groups, as well as small amounts of indene derivatives. The distributions of product molecules are demonstrated in Fig. 1 and the GC-MS spectra are displayed in Fig. S1.

When ethylene is reacted with methane, compared with the control group run under  $N_2$  environment, the molar fractions of benzene and toluene among the product molecules are lower, while the fractions of C<sub>8</sub>–C<sub>13</sub> groups are increased (Fig. 1a). Such a shift of product distribution towards larger carbon number species suggests the incorporation of an extra carbon source, i.e., methane, into the product molecules. The shift becomes more significant when 1-butene is employed as the olefin feedstock (Fig. 1b), indicating that participation of methane is pronounced. This effect becomes even more pronounced when 1-hexene is introduced to react with methane (Fig. 1c), but diminishes when 1-octene and 1-decene are used as the olefin feedstocks. The general aromatic products distribution shift towards the higher end observed under a methane environment may suggest the incorporation of the methane carbon resulting from its activation with the facilitation of the charged catalyst. In the reaction matrix presented in this work, the aromatization processes of alkane and alkene molecules are involved, where the activation of methane, alkene isomerization, oligomerization and cracking, and alkene aromatization through cyclization and hydrogen transfer take place. As an alkane molecule, the activation of methane might follow two routes including protolytic cracking and hydrogen transfer between methane and the product alkenes [55–57]. The methane activation and conversion improvement in the presence of co-fed hydrocarbon molecules observed in this work as well as other literature suggest that the step involving multiple molecules, i.e., hydrogen transfer, could play a more critical role. In a hydrogen transfer

**Table 1**

The average carbon number, substitution index and aromatic carbon fraction of products obtained from the reaction between olefins and CH<sub>4</sub> over Ag-Ga/HZSM-5 catalysts at 400 °C and 5.0 MPa.

Olefin Feedstock	C <sub>2</sub> H <sub>4</sub>		C <sub>4</sub> H <sub>8</sub>		C <sub>6</sub> H <sub>12</sub>		C <sub>8</sub> H <sub>16</sub>		C <sub>10</sub> H <sub>20</sub>	
Gas Environment	N <sub>2</sub>	CH <sub>4</sub>	N <sub>2</sub>	CH <sub>4</sub>	N <sub>2</sub>	CH <sub>4</sub>	N <sub>2</sub>	CH <sub>4</sub>	N <sub>2</sub>	CH <sub>4</sub>
Average Carbon Number	8.61	8.67	8.34	8.69	7.68	8.62	8.12	8.30	8.05	8.06
Substitution Index	0.260	0.269	0.245	0.268	0.202	0.234	0.216	0.230	0.213	0.214
Aromatic Carbon Fraction	0.750	0.743	0.764	0.742	0.798	0.775	0.782	0.774	0.791	0.787

step, a carbenium cation, which could originate from the reaction between acidic sites on the catalyst surface and olefin molecules, can react with an alkane molecule, such as CH<sub>4</sub>. Through H-transfer, new carbenium cations like CH<sub>3</sub><sup>+</sup> are produced, which might participate in the aromatization reaction and incorporate into product molecules. The spatial requirement, however, has to be met to allow the bimolecular H-transfer step to take place and this would have a profound effect on the aromatization process [37]. The most outstanding averaged aromatic products carbon number increment is witnessed when 1-hexene is employed as the olefin feedstock, suggesting that the molecular size difference also has a significant effect on the co-aromatization reaction. This response to the spatial effect, therefore, implies that the co-aromatization taking place in the inner pores dominates the reaction compared with that on the external surface.

To get a more accurate evaluation on the methane participation, parameters including the averaged carbon number, the substitution index and the aromatic carbon fraction of all product molecules are calculated (Table 1 and Fig. S2). The average carbon number of product molecules is calculated based on the molar fraction of product molecules with variable carbon numbers. The substitution index demonstrates the fraction of carbon atoms that are attached to substitute groups among the phenyl ring carbon atoms in the product molecules. The aromatic carbon fraction is the fraction of carbon atoms on the phenyl rings among all the carbon atoms in the product matrix. Under a methane environment, not only the average carbon number is increased, which is consistent with the aforementioned product

distribution shift towards larger carbon number products, but escalated substitution index along with a reduced aromatic carbon number are also witnessed, suggesting that in the presence of methane, more side chain groups are attached to the phenyl rings during the aromatization process. These additional side chains might be contributed by, but not limited to the CH<sub>3</sub><sup>+</sup> species upon methane activation and C–H bond cleavage. When 1-hexene is the reactant, the greatest increments in terms of average carbon number (7.68–8.62) as well as the substitution index (0.202–0.234), and the largest reduction of aromatic carbon fraction (0.798–0.775) are observed when CH<sub>4</sub> is introduced compared with its N<sub>2</sub> counterpart, indicating the greatest participation of methane in this reaction matrix.

### 3.2. Methane participation evidenced by <sup>13</sup>C labelling

The direct evidence of methane participation in the co-aromatization reaction is observed in the NMR spectra when <sup>13</sup>C-labelled methane is introduced as gas feedstock. Fig. 2 displays the <sup>13</sup>C NMR spectra of the liquid products when CH<sub>4</sub> and <sup>13</sup>CH<sub>4</sub> are employed as the methane source to react with ethylene, 1-butene, 1-hexene, 1-octene and 1-decene under the facilitation of Ag-Ga/ZSM-5 catalyst. Combining with the product distribution obtained from GC–MS analysis and the <sup>13</sup>C chemical shift of variable carbons sites [58], the peaks between 124–137 ppm are assigned to carbon sites on the phenyl rings, while those between 14–35 ppm are attributed to carbon sites of the alkyl side chains. The aromatic carbon NMR signals can be divided into three

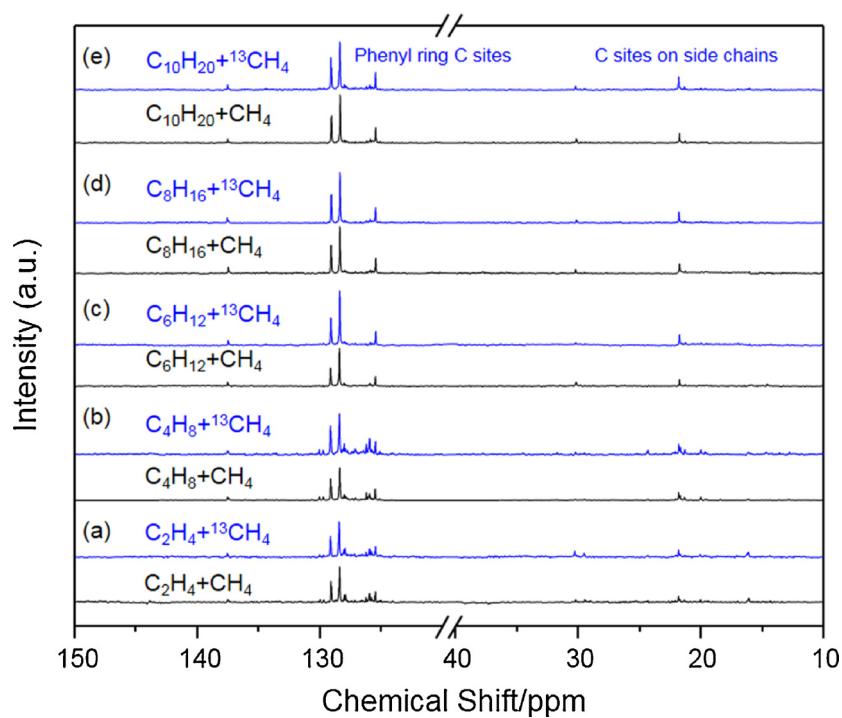


Fig. 2. The <sup>13</sup>C NMR spectra of the liquid products collected from the reaction between olefins and CH<sub>4</sub>/<sup>13</sup>CH<sub>4</sub> over Ag-Ga/HZSM-5 at 400 °C and 0.3 MPa.

**Table 2**

The increased  $^{13}\text{C}$  NMR peak area percentage of the aromatization products with different olefins under  $^{13}\text{CH}_4$  environment compared with those from  $\text{CH}_4$  counterpart at 400 °C and 0.3 MPa.

Olefin Feedstock	Ethylene	1-Butene	1-Hexene	1-Octene	1-Decene
Phenyl ring carbon	3	21	32	10	4
Alkyl carbon	54	53	42	21	31

groups. The peaks around 137 ppm are due to the phenyl carbon sites that are bonded to alkyl substituent groups. The peaks that appear between 128–130 ppm are assigned to the phenyl ring carbon atoms that are on the ortho and meta positions of the alkyl substituent, while the others in the region of 124–127 ppm are due to the para carbon sites. The peak area increment values using  $^{13}\text{CH}_4$  compared with those from its non-isotope labelled counterpart, where the peak areas due to the  $\text{CS}_2$  solvent are used as the internal reference, are listed in Table 2. During  $^{13}\text{C}$  NMR measurement, in order to collect a large number of scans to improve the quality of the spectra, the recycle delay is not set long enough for all the excited  $^{13}\text{C}$  nuclei to relax to ground state. As a result, the peak area may not be linearly proportional to the concentration of  $^{13}\text{C}$  in the products. However, the significantly escalated peak areas strongly indicate the  $^{13}\text{C}$  enrichment under  $^{13}\text{CH}_4$  environment, resulting from the methane participation in the aromatization reaction. When ethylene is reacting with  $^{13}\text{CH}_4$ , peak area increment due to alkyl side chain carbon sites is more significant than phenyl ring carbon sites. It might be because the incorporation of methane carbon atoms into the substitution groups is more feasible to take place than the phenyl ring formation step. There might be some requirements regarding the reaction intermediate molecules during the phenyl ring formation process in the inner pores. One possible explanation is that the reaction intermediate formed from methane and ethylene is less reactive in phenyl ring formation, compared with other olefin feedstocks. A similar phenomenon is observed when 1-butene and 1-hexene are the feedstocks, while the  $^{13}\text{C}$  peak area increment of the phenyl ring carbons under  $^{13}\text{CH}_4$  condition is getting larger, suggesting an enhanced participation in the phenyl ring formation step. However, as the olefin feedstocks are 1-octene and 1-decene, the  $^{13}\text{C}$  enrichment in phenyl rings declines significantly. This phenomenon implies that the effect of feedstock molecule size is more decisive for the methane participation in the phenyl ring formation step. A possible conjecture is that the aromatization step mainly takes place on the inner pore catalytic sites and some spatial requirement related to the co-aromatization feedstock must be met to allow the methane participation, whereas the incorporation of methane into substitute groups depends less on these sites.

### 3.3. Methane co-aromatization with olefins over Ag-Ga/HY

It has been demonstrated from the aforementioned study that the methane participation diminishes as the co-fed olefin molecule gets larger from 1-hexene to 1-octene and 1-decene, which might be attributed to that the increased olefin molecular size leaves less room for the methane molecule to be present in the inner pore along with the pre-charged olefin molecule and carry out the co-aromatization reaction. To appreciate this hypothesis, HY, which bears larger inner pores than HZSM-5, is engaged as the catalyst support material. The co-aromatization reactions of 1-hexene, 1-octene and 1-decene with methane are again practiced over Ag-Ga/HY catalyst and compared with their  $\text{N}_2$  environment counterparts (Fig. S3 and S4).  $\text{C}_8$  and  $\text{C}_9$  products are the major products obtained from  $\text{N}_2$  runs, which might be attributed to the self-aromatization of the charged olefins. Compared with the  $\text{C}_7$  and  $\text{C}_8$  dominated aromatic products witnessed over Ag-Ga/HZSM-5 in the aforementioned study, the enhanced product molecular size from Ag-Ga/HY catalyst can be explained by the larger pore size of HY support

**Table 3**

The average carbon number, substitution index and aromatic carbon fraction of products obtained from the reaction between olefins and  $\text{CH}_4$  over Ag-Ga/HY catalysts at 400 °C and 5.0 MPa.

Olefin Feedstock	$\text{C}_6\text{H}_{12}$		$\text{C}_8\text{H}_{16}$		$\text{C}_{10}\text{H}_{20}$	
	$\text{N}_2$	$\text{CH}_4$	$\text{N}_2$	$\text{CH}_4$	$\text{N}_2$	$\text{CH}_4$
Average Carbon Number	8.67	9.08	8.56	8.73	8.89	9.32
Substitution Index	0.306	0.339	0.286	0.332	0.347	0.395
Aromatic Carbon Fraction	0.744	0.728	0.762	0.740	0.720	0.689

that curtails the diffusion limitation of and allows more room to hold these larger product molecules. Under methane environment, the major products are shifted to  $\text{C}_9$  and  $\text{C}_{10}$  products, accompanied by increased average carbon number, larger substitution index and reduced aromatic carbon fraction (Table 3 and Fig. S5). It is worth noting that these changes are similar when different olefins feedstocks are used, despite the smaller methane conversion observed when larger olefin molecules are engaged (Table S1). A plausible explanation is that the larger inner pore of zeolite Y support lessens the diffusion barrier of large molecules and gives more room for the co-aromatization between the olefin species and methane molecules within the inner pores. Therefore, the extent of methane participation is less dependent on the molecular size of the olefin feedstocks if HY is used as the zeolite support compared with that for the co-aromatization using Ag-Ga/HZSM-5 catalysts.

### 3.4. Contribution by catalytic sites in the inner pores and on the external surface

The contribution of the catalytic sites located in the inner pores and the external surface of the catalyst is systematically evaluated by manipulating the amount of these catalytic sites and monitoring the change made to product distribution. ZSM-5, the support material of the Ag-Ga/HZSM-5 employed in the aforementioned reactions, is treated by NaOH aqueous solution to introduce mesopores to the structure [53], leading to the formation of a micro/meso pore hierarchical structure and thus increased external surface area. The catalyst prepared with this modified support after loading Ag and Ga species is denoted Ag-Ga/HZSM-5 (hierarchical). As is displayed in Fig. 3, the treatment introduces additional pores to the external surface of the particles, resulting in decreased microporous surface area in the inner pores (Table 4). However, the fringe of ZSM-5 is still observed (Fig. 3b), indicating the ZSM-5 structure remains intact. The co-aromatization of methane and 1-hexene is carried out and compared with its counterpart under  $\text{N}_2$  environment. The product distribution is demonstrated on the GC-MS spectra (Fig. S6). Parameters including the average carbon number, the substitution index and the aromatic carbon fraction are listed in Table 5 and Fig. S7. Compared with the products from conventional Ag-Ga/HZSM-5 when  $\text{N}_2$  is the gas phase, the formation of larger aromatic molecules such as ethylbenzene, xylene and  $\text{C}_9\text{-C}_{11}$  products is enhanced when Ag-Ga/HZSM-5 (hierarchical) is charged, resulting in an increased carbon number and substitution index accompanied by decreased aromatic carbon fraction. This observation shows that the external catalytic sites favor the formation of larger aromatization products, while those in the inner pores are mainly responsible for smaller ones, which can be attributed to the diffusion limitation as well as the spatial constraint to the reaction intermediates towards the formation of aromatic products with larger molecular size [33,34,42,43]. When the reaction is carried out under  $\text{CH}_4$  over Ag-Ga/HZSM-5 (hierarchical), increased average carbon number, enhanced substitution index and decreased aromatic carbon fractions are witnessed, which might be attributed to methane participation in the aromatization process. These changes due to  $\text{CH}_4$  introduction, however, are not as significant as those observed on conventional Ag-Ga/HZSM-5. For instance, the average carbon number is increased from 7.68 to

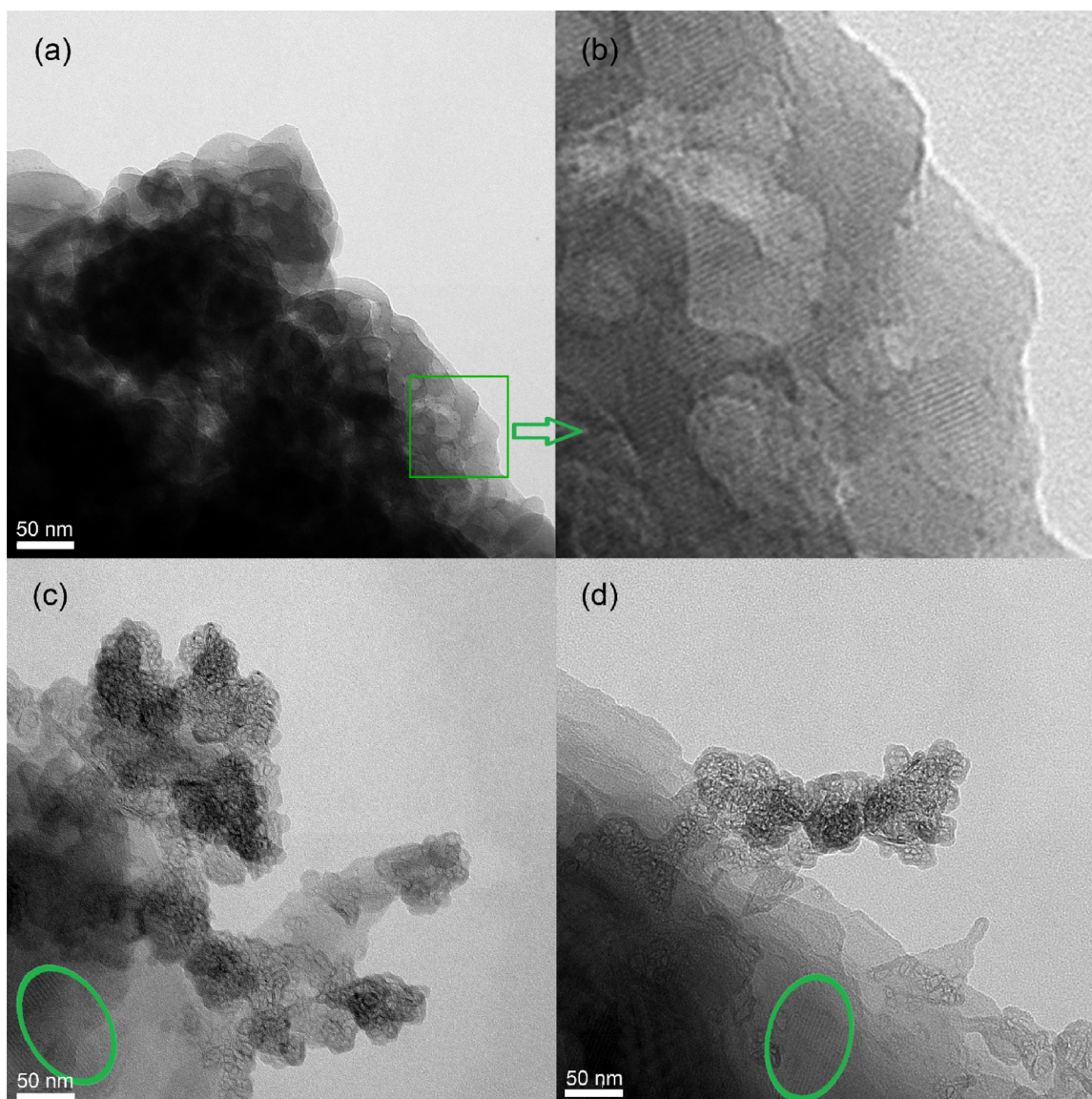


**Fig. 3.** The TEM images of Ag-Ga/HZSM-5 (hierarchical) (a and b) and Ag-Ga/HZSM-5 (nanosize) (c and d). The ZSM-5 fringes are highlighted in green circles (For interpretation of the references to colour in this figure legend, the reader is referred to the web version of this article).

**Table 4**  
The porous properties of various catalysts.

	BET Surface Area ( $\text{m}^2/\text{g}$ )		
	External	Microporous	Total
HZSM-5	109	292	401
HZSM-5 (nanosize)	175	189	364
Ag-Ga/HZSM-5	108	346	454
Ag-Ga/HZSM-5 (nanosize)	163	180	343
Ag-Ga/HZSM-5/SiO <sub>2</sub>	78	290	368
Ag-Ga/ZSM-5 (hierarchical)	106	192	298
Ag-Ga/ZSM-5 (inner pore blocked)	103	158	261
HY	196	725	921
Ag-Ga/HY	233	659	892

8.62 when  $\text{CH}_4$  is employed compared with its  $\text{N}_2$  counterpart over conventional Ag-Ga/HZSM-5. However, this increment is only 0.35, from 8.20 to 8.55, when Ag-Ga/HZSM-5 (hierarchical) is charged as the catalyst. The substitution increment (0.252–0.281), however, is similar to that of conventional Ag-Ga/HZSM-5 (0.202–0.234).

Another method to modify the ratio between the external surface

and inner pore surface areas is to change the particle size of the catalysts. Nanosize ZSM-5 is synthesized and employed to prepare the Ag-Ga/HZSM-5 (nanosize) catalysts. The nanosize ZSM-5 aggregates consist of particles around 50 nm with ZSM-5 fringes visible in the TEM images (Fig. 3). The reduced particle size of catalyst particles increases the external surface area while decreasing the microporous surface area of the inner pores, compared with that of Ag-Ga/HZSM-5 prepared with conventional ZSM-5 (Table 4). Comparison to the co-aromatization products with those from conventional Ag-Ga/HZSM-5 shows the altered methane participation pathway when more external surface is present, which is similar to the phenomena observed over Ag-Ga/HZSM-5 (hierarchical). During the co-aromatization with propane over Ag-Ga/HZSM-5 (nanosize), methane participation suppresses the formation of naphthalene derivatives, while enhancing the production of mono-aromatics with multiple branches (Fig. S6). As a result, the average carbon number is slightly increased, the substitution index is increased and the aromatic carbon fraction is decreased (Table 5).

These phenomena are further evaluated by blocking the inner pores with coke deposits owing to the significantly improved coke formation rate in the inner pores over Ca-ZSM-5 [46]. After the inner pores are blocked, the remaining Ca sites are converted to hydroxyl sites by ion-

**Table 5**

The average carbon number, substitution index and aromatic carbon fraction of products obtained from the reaction between 1-hexene and CH<sub>4</sub> over Ag-Ga/HZSM-5, Ag-Ga/HZSM-5 (micro/meso pore hierarchical structure) and Ag-Ga/HZSM-5 (inner pore blocked) catalysts at 400 °C and 5.0 MPa.

Post-synthetic Treatments	SiO <sub>2</sub>		Conventional		Hierarchical		Nanosize		Inner pore blocked	
	N <sub>2</sub>	CH <sub>4</sub>	N <sub>2</sub>	CH <sub>4</sub>	N <sub>2</sub>	CH <sub>4</sub>	N <sub>2</sub>	CH <sub>4</sub>	N <sub>2</sub>	CH <sub>4</sub>
Average Carbon Number	7.75	8.39	7.86	8.62	8.20	8.55	8.62	8.69	8.35	8.50
Substitution Index	0.195	0.206	0.202	0.234	0.252	0.281	0.214	0.235	0.268	0.291
Aromatic Carbon Fraction	0.808	0.792	0.798	0.775	0.757	0.740	0.792	0.778	0.751	0.733

exchange with NH<sub>4</sub>NO<sub>3</sub> (aq) and calcination under N<sub>2</sub> environment. The coke deposit in the inner pores may cover the Ca<sup>2+</sup> cations and prevent them from NH<sub>4</sub><sup>+</sup> exchange. The BET surface areas including the microporous surface areas and the external surface areas of the catalysts are measured and included (Table 4). By depositing coke to the inner pores, the microporous surface area of Ag-Ga/HZSM-5 is reduced by 46% from 292 to 158 m<sup>2</sup>/g. The external surface area, on the other hand, is not significantly changed. The BET analysis results suggest that the coke deposit is mainly in the inner pores.

In order to better justify the feasibility of the inner pore coke deposit approach, Scanning Transmission X-ray Microscopy (STXM) is utilized to track the location of coke deposits. STXM has been employed as a technique that could map the elemental distribution on particles by many other research groups. For instance, Wang et al. [54] collected the Zn STXM images to probe the Zn species in the ZnS/ZnO nano-heterostructure. The different environment of Zn when bonded to O or S made it possible to differentiate ZnS and ZnO in the same particle. Remusat et al. [59] employed STXM as a transmission technique, which averages information over the entire thickness of the sample in a 5 μm wide region, to detect and locate organic species. In the present work, the signal of carbon is too weak because the coke deposit is made of carbon atoms with diverse chemical environments resulting in a low signal to noise ratio. Therefore, a different strategy was employed by focusing on the signal of Ca atoms. After coke deposit step in the present work, there should be two kinds of Ca species. Some Ca atoms are buried in the coke deposit, while some are not. Those buried in coke cannot be removed by NH<sub>4</sub><sup>+</sup> ion-exchange following the coke deposit step. As a result, the presence of Ca remaining in the ZSM-5 framework is associated with the presence of coke deposits. Therefore, a higher concentration of Ca in certain regions in the particle indicates the presence of coke deposit. Fig. 4 shows the STXM image of the Ca-ZSM-5 particles. The XANES spectra at the Ca L edge of the Ca species located

in the middle and on the edge of the particles are also displayed. The peak around 348.5 eV is due to L<sub>3</sub> edge while the peak around 351.5 eV is assigned to L<sub>2</sub> edge adsorption. The Ca signal collected in a small area in the middle of the particle, where the Ca species is mainly within the inner pores, is significantly stronger compared with that collected from the Ca species from a much larger area on the edge of the particles, where there are more Ca species located on or close to the external surface. These observations suggest that the Ca concentration is much higher within inner pores, while the Ca signal is weak on the external surface. This phenomenon probably results from the fact the inner pores are blocked by coke deposit. As a result, the Ca species are covered by coke and cannot be ion-exchanged by NH<sub>4</sub><sup>+</sup> cations. Ag-Ga/HZSM-5 with inner pores blocked is thus prepared using the obtained support material. The microporous surface area in the inner pores is significantly reduced compared with the conventional Ag-Ga/HZSM-5 catalyst.

Its catalytic performance is compared with that over conventional Ag-Ga/HZSM-5 in terms of product distribution (Table 5 and Figs. S6–S7). With the inner pore sites blocked and only external sites remaining, the effect on the product distribution is similar to but still more significant comparing with that observed over Ag-Ga/HZSM-5 (hierarchical). For instance, the average carbon number of products from N<sub>2</sub> condition is escalated from 8.20 to 8.50. The contribution of methane on the product distribution shift is further suppressed. The average carbon number increment under CH<sub>4</sub> is only 0.15 (8.35–8.50). On the other hand, Ag-Ga/HZSM-5/SiO<sub>2</sub>, where the external acid sites are deactivated by SiO<sub>2</sub> covering, is used as the catalyst to study the contribution of inner pore catalytic sites. The microporous surface area of the Ag-Ga/HZSM-5/SiO<sub>2</sub> is similar to that of conventional Ag-Ga/HZMS-5, indicating that the treatment does not noticeably block the inner pores. This is further evidenced by molecular simulation. The diameter of the (3-aminopropyl)triethoxysilane molecule, which is the

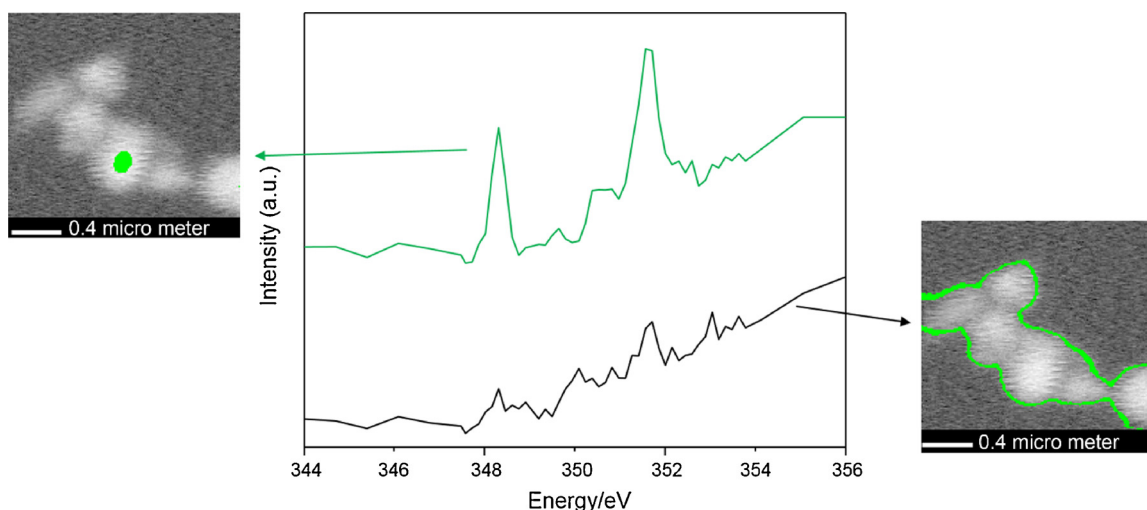


**Fig. 4.** STXM images of HZSM-5 (inner pore blocked) particles and the XANES spectra of the Ca species located in the middle (image on the left, green curve on the top) and on the edge (image on the right, black curve at the bottom) of the HZSM-5 particles (For interpretation of the references to colour in this figure legend, the reader is referred to the web version of this article).

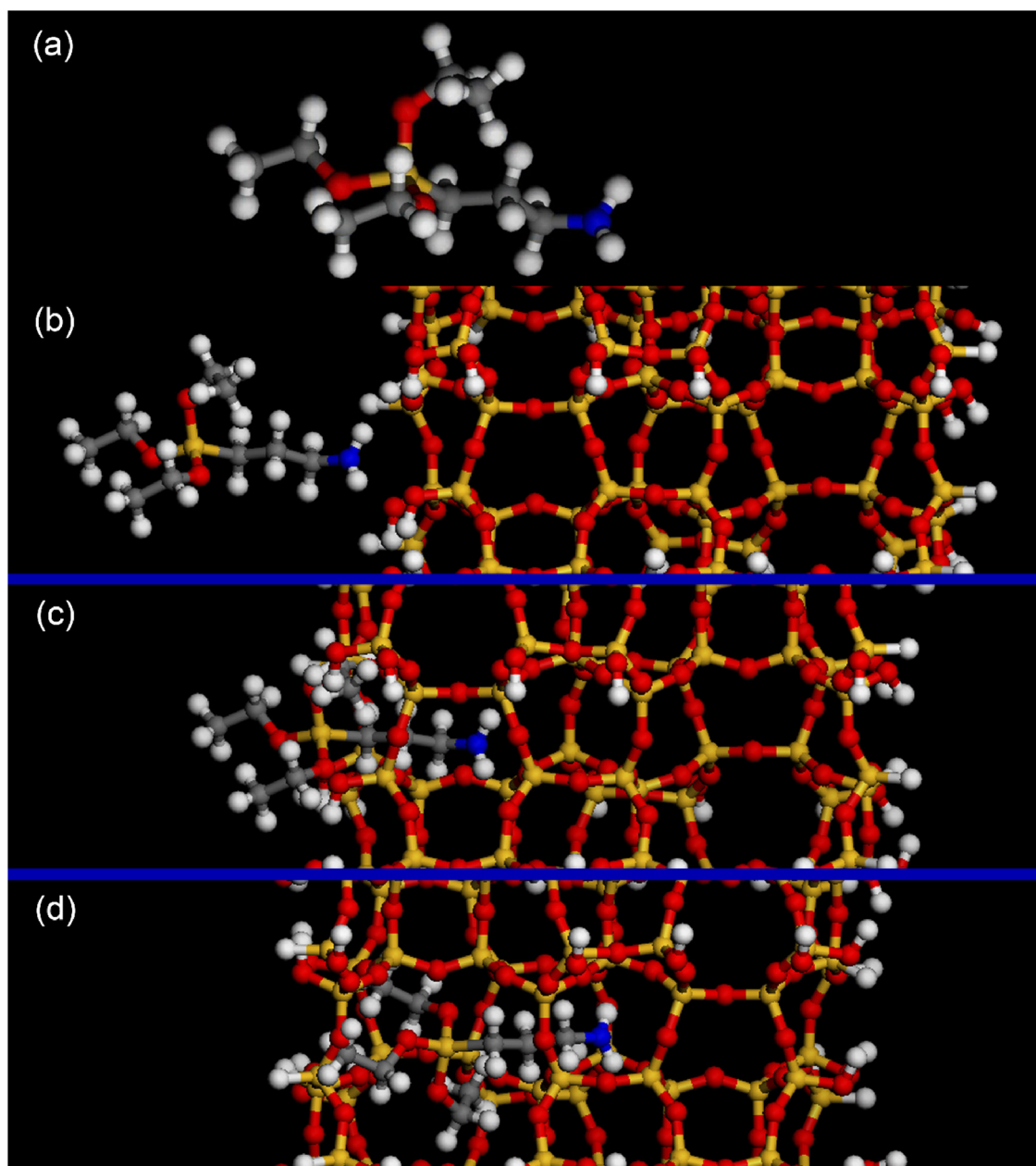


**Fig. 5.** The optimized structure of the (3-aminopropyl)triethoxysilane molecule (a) and the locations of the molecule with respect to ZSM-5 framework (b–d).

precursor of the SiO<sub>2</sub> species that cover the acid sites on the external surface of the catalyst, is determined to be 11.9 Å by theoretical calculation (Fig. 5a). This diameter is much larger than the pore size of ZSM-5 (5.6 Å), making it difficult to enter the inner pores of the ZSM-5 framework. As a result, the energy of system is greatly increased if the molecule enters into ZSM-5 tunnels and inner pores. The adsorption energy is estimated as –5.2 kJ/mol when the (3-aminopropyl)triethoxysilane molecule lays on the external surface (Fig. 5b). If this molecule enters into the tunnels (Fig. 5c) and the inner pores (Fig. 5d) of ZSM-5, the adsorption energy is greatly increased to 8246.0 and 8746.1 kJ/mole, respectively. The high energy of these states demonstrate that the inner pore diffusion of this molecule is not favorable. These observations confirm that (3-aminopropyl)triethoxysilane, the precursor molecule of SiO<sub>2</sub>, might only react with the catalytic sites on the external surface of the catalysts.

Comparing with the product distribution with that obtained with conventional Ag-Ga/HZSM-5 under N<sub>2</sub> environment, the formation of large aromatics (C<sub>8</sub>–C<sub>12</sub>) is suppressed. Under CH<sub>4</sub> condition, the

formation of these species is enhanced, particularly naphthalene derivatives (C<sub>10</sub>–C<sub>12</sub>), resulting in greatly increased average carbon number but modest substitution index increment. The products with multiple sidechains such as C<sub>8</sub> and C<sub>9</sub> are not increased as great, indicating that the substitution group addition capacity of the inner pore sites are not as effective as the external ones. In summary, the inner pore catalytic sites favor the formation of light aromatic products, while the presence of external sites pronounces the selectivity of large aromatics with substitution groups. When methane takes part in the co-aromatization process, the catalytic sites in the inner pores play a critical role in the co-aromatization of methane and 1-hexene, particularly the phenyl ring formation step, whereas the external ones have a more profound effect on the substitution groups addition to the aromatic products.

The co-aromatization products with CH<sub>4</sub> and <sup>13</sup>CH<sub>4</sub> over these catalysts are analyzed using <sup>13</sup>C NMR (Fig. 6) to get a more comprehensive understanding of the contribution of catalytic sites in the inner pores and on the external surfaces. The peak area increments when <sup>13</sup>C-enriched methane is used are listed in Table 6. Compared with the

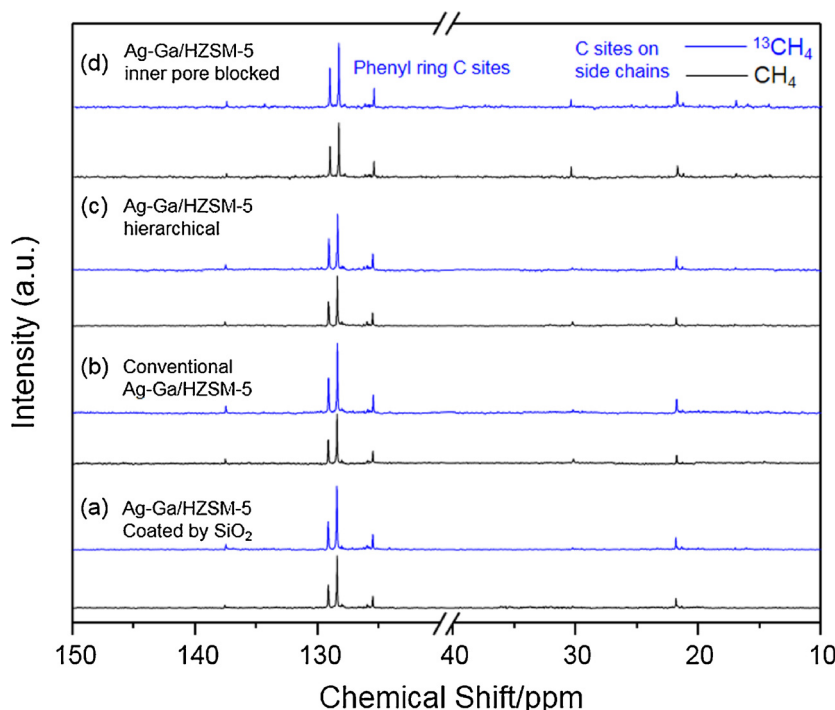


**Fig. 6.** The  $^{13}\text{C}$  NMR spectra of the liquid products collected from the reaction between 1-hexene and  $\text{CH}_4/^{13}\text{CH}_4$  over Ag-Ga/HZSM-5/SiO<sub>2</sub> (a), conventional Ag-Ga/HZSM-5 (b), Ag-Ga/HZSM-5 (micro/meso pore hierarchical structure) (c) and Ag-Ga/HZSM-5 (inner pore blocked) (d) at 400 °C and 0.3 MPa.

**Table 6**

The increased  $^{13}\text{C}$  NMR peak area percentage of the aromatization products obtained from 1-hexene and  $\text{CH}_4/^{13}\text{CH}_4$  over Ag-Ga/HZSM-5/SiO<sub>2</sub>, conventional Ag-Ga/HZSM-5, Ag-Ga/HZSM-5 (micro/meso pore hierarchical structure) and Ag-Ga/HZSM-5 (inner pore blocked) at 400 °C and 0.3 MPa.

Catalyst	Ag-Ga/HZSM-5 /SiO <sub>2</sub>	Ag-Ga/HZSM-5	Ag-Ga/HZSM-5 (hierarchical)	Ag-Ga/HZSM-5 (inner pore blocked)
Phenyl ring carbon	39	32	23	11
Alkyl carbon	38	42	68	50

results of products from conventional Ag-Ga/HZSM-5, when the external sites are covered by coated SiO<sub>2</sub>, the peak area increments of substitution alkyl sites is decreased accompanied with the notable increase at phenyl ring carbon sites. This observation indicates that the external catalytic sites prefer to make contribution to the methane participation in the substitution alkyl groups. When additional external surface sites are introduced by the micro/meso pore hierarchical structure, the phenyl ring carbon peak area increment is decreased from 32% to 23%, while that of substitution alkyl sites is increased from 42% to 68% when compared with the conventional Ag-Ga/HZSM-5. A similar trend is also observed when the inner pore of the catalyst is blocked. These phenomena further demonstrate that the external catalytic sites favor for methane participation into the substitution alkyl groups, while the catalytic sites in the inner pores mainly contribute to the incorporation of methane carbon atoms into the phenyl rings.

### 3.5. Methane activation investigation using $^2\text{D}$ isotope labelling by NMR

Besides  $^{13}\text{CH}_4$ , deuterium-enriched methane, CD<sub>4</sub>, is also used as the methane source in the co-aromatization reaction in order to study the C–H activation of methane molecules during this process. The  $^1\text{H}$  and  $^2\text{D}$  NMR spectra of the 1-hexene and CD<sub>4</sub> co-aromatization products are acquired and compared with those collected over their non-isotopic counterpart, where the catalysts are Ag-Ga/HZSM-5/SiO<sub>2</sub>, conventional Ag-Ga/HZSM-5, Ag-Ga/HZSM-5 (micro/meso pore hierarchical structure) and Ag-Ga/HZSM-5 (inner pore blocked), respectively. On the  $^1\text{H}$  NMR spectra (Fig. S8), the peaks at 7.24 ppm are due to the CHCl<sub>3</sub> in the solvent, the intensities of which are similar when CH<sub>4</sub> and CD<sub>4</sub> are

reacted. The intensities of other peaks, however, are suppressed significantly when CD<sub>4</sub> is present in the reaction. The peaks between 6.9–7.8 ppm are due to the H atoms on the phenyl rings. The signals between 2.0–2.8 ppm can be assigned to benzylic H sites. Those appearing at the region below 2 ppm are attributed to H sites of the alkyl groups that are not bonded to phenyl rings directly. The ratios between the peak areas with respect to that of CHCl<sub>3</sub> are shown in Table 7. The signals, especially those due to phenyl aromatic and benzylic H sites, are greatly reduced in the isotopic labelled products, implying that methane hydrogens favor the aromatic and benzylic hydrogen sites over the alkyl group hydrogen sites. The percentage of D atoms in the phenyl rings of the products from Ag-Ga/HZSM-5 (inner pore blocked), however, is similar with that of conventional Ag-Ga/HZSM-5. This might be because that high percentage of D in phenyl rings may be contributed by other processes besides the methane incorporation in the reaction itself. For instance, the H/D exchange may be feasible at the phenyl ring hydrogen sites. Therefore, the difference due to methane participation in the phenyl ring formation step does not stand out. The incorporation of D from methane into the products is further confirmed by the  $^2\text{D}$  NMR spectra (Fig. 7). When the external catalytic sites are covered by SiO<sub>2</sub>, the incorporation of D to the phenyl ring and benzylic hydrogen sites are more significant compared with the conventional Ag-Ga/HZSM-5 catalyst (Table 7). Blocking the inner pores, on the other hand, promotes the D atom incorporation into the alkyl hydrogen sites on the side chains, resulting in much stronger  $^2\text{D}$  NMR signals due to these sites (Fig. 7d). However, the incorporation into the phenyl rings remains almost unchanged comparing with that from conventional Ag-Ga/HZSM-5, indicating that the catalytic sites on the external surface

**Table 7**

Peak area reduction percentage of the aromatization products of 1-hexene and CD<sub>4</sub> over Ag-Ga/HZSM-5/SiO<sub>2</sub>, conventional Ag-Ga/HZSM-5, Ag-Ga/HZSM-5 (micro/meso pore hierarchical structure) and Ag-Ga/HZSM-5 (inner pore blocked) catalysts compared with non-isotope labelling counterparts at 400 °C and 0.3 MPa.

H/D sites	Ag-Ga/HZSM-5 /SiO <sub>2</sub>	Ag-Ga/HZSM-5	Ag-Ga/HZSM-5 (hierarchical)	Ag-Ga/HZSM-5 (inner pore blocked)
Phenyl ring	65	51	53	54
Benzyllic	49	35	36	32
Alkyl	4	3	1	17

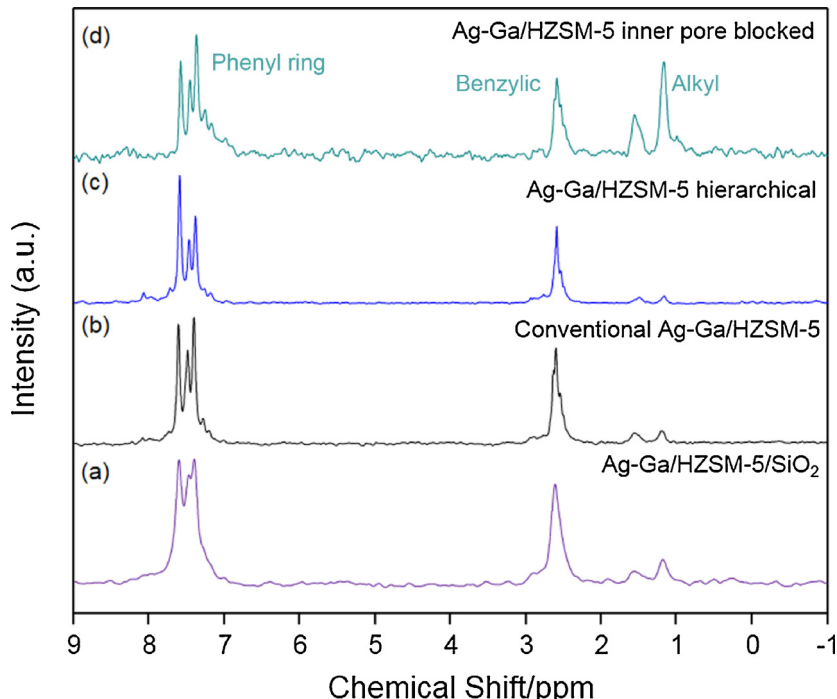


**Fig. 7.** The <sup>2</sup>D NMR spectra of the co-aromatization products collected from the reaction between 1-hexene and CD<sub>4</sub> over Ag-Ga/HZSM-5/SiO<sub>2</sub> (a), conventional Ag-Ga/HZSM-5 (b), Ag-Ga/HZSM-5 (micro/meso pore hierarchical structure) (c) and Ag-Ga/HZSM-5 (inner pore blocked) (d) at 400 °C and 0.3 MPa.

would prefer to catalyze the incorporation of D atoms from methane into the side chains rather than into the phenyl rings. The NMR analysis of the co-aromatization products obtained from conventional Ag-Ga/HZSM-5, where the co-fed olefin feedstocks are 1-octene (Fig. S10) and 1-decene (Fig. S11) in addition to 1-hexene (Fig. S9), is also carried out. The <sup>1</sup>H NMR peaks areas are displayed in Table S2. It is worth noting that when the co-fed olefin feedstock molecule gets larger to 1-octene and 1-decene, the peak D atom incorporation to the side chain alkyl sites is significantly enhanced. The diffusion limitation due to the increased olefin molecular size might suppress the D atom participation into the phenyl rings within the pores, while allowing the participation to take place on the external catalytic sites, resulting in pronounced D substitution into the side chain hydrogen sites. For the incorporation of D atoms, there may exist additional pathways, for instance, H/D exchange, which can occur upon the activation of methane over hydroxyl groups [23,28], besides its incorporation along with methane carbon atoms. Compared with the peak area change observed on the <sup>13</sup>C NMR spectra, the involvement of hydrogen is far more profound than carbon from the methane molecules, indicating the selective D incorporation over different catalytic sites might mainly result from their different C–H bond activation capacity.

#### 4. Conclusions

The work presented here investigates the co-aromatization of methane with olefin feedstocks over Ag and Ga modified zeolite based catalysts. When Ag-Ga/HZSM-5 is used as the catalyst, the methane

participation into the co-aromatization products with ethylene, 1-butene, 1-hexene, 1-octene and 1-decene, in terms of increased average carbon number and diffusion index and decreased aromatic carbon fraction of the formed aromatic products, is witnessed. As the olefin feedstock gets larger in molecular size from 1-hexene to 1-octene and 1-decene, the participation of methane diminishes, which is also evidenced by the <sup>13</sup>C isotope labelling. This difference among various olefin feedstocks becomes less significant when Ag-Ga/HY is employed as the catalyst, suggesting that the variation in methane participation degree might originate from the pore size constraint of the charged catalyst. The role played by the catalytic sites in the inner pores and on the external surface is further investigated by engaging different ZSM-5 support materials. When only inner pore sites are available, the aromatization product is mainly composed of light aromatics including benzene and toluene. The presence of external catalytic sites would enhance the formation of larger aromatic products, which becomes more significant as more external catalytic sites are available. The methane participation into the co-aromatization reaction occurs on both inner pore and external catalytic sites. The presence of inner pore catalytic sites might mainly contribute to the incorporation of methane into phenyl rings of the formed aromatics, whereas the external ones tend to be more related to the facilitation of the methane's incorporation into the substitution groups of the produced aromatic compounds, which is consistent with the observations on <sup>13</sup>C and <sup>2</sup>D NMR spectra.

## Acknowledgements

We gratefully acknowledge the financial supports from Shandong Chambroad Petrochemicals Co. Ltd. as well as Meg Energy Corp. and Alberta Innovates - Energy and Environment Solutions (AI-EES, 2142). We appreciate the XAS facilities provided by the Canadian Light Source. We thank Dr. Zhiqiang Wang for his guidance in the analysis of the XAS data.

## Appendix A. Supplementary data

Supplementary material related to this article can be found, in the online version, at doi:<https://doi.org/10.1016/j.apcatb.2018.04.034>.

## References

- [1] J.H. Lunsford, The catalytic oxidative coupling of methane, *Angew. Chem. Int. Ed.* 34 (1995) 970–980, <http://dx.doi.org/10.1002/anie.199509701>.
- [2] Y. Amenomiya, V.I. Birss, M. Goledzinowski, J. Galuszka, A.R. Sanger, Conversion of methane by oxidative coupling, *Catal. Rev.* 32 (1990) 163–227, [http://dx.doi.org/01614949009351351](http://dx.doi.org/10.1080/01614949009351351).
- [3] U. Zavyalova, M. Holena, R. Schlägl, M. Baerns, Statistical analysis of past catalytic data on oxidative methane coupling for new insights into the composition of high-performance catalysts, *ChemCatChem* 3 (2011) 1935–1947, <http://dx.doi.org/10.1002/cctc.201100186>.
- [4] C. Li, C. Dinoi, Y. Coppel, M. Etienne, CH bond activation of methane by a transient  $\eta$  2-cyclopropane-metallabicyclobutane complex of niobium, *J. Am. Chem. Soc.* 137 (2015) 12450–12453, <http://dx.doi.org/10.1021/jacs.5b07859>.
- [5] Y. Cui, Y. Xu, J. Lu, Y. Suzuki, Z.G. Zhang, The effect of zeolite particle size on the activity of Mo/HZSM-5 in non-oxidative methane dehydroaromatization, *Appl. Catal. A Gen.* 393 (2011) 348–358, <http://dx.doi.org/10.1016/j.apcata.2010.12.017>.
- [6] Y. Xu, X. Bao, L. Lin, Direct conversion of methane under nonoxidative conditions, *J. Catal.* 216 (2003) 386–395, [http://dx.doi.org/10.1016/S0021-9517\(02\)00124-0](http://dx.doi.org/10.1016/S0021-9517(02)00124-0).
- [7] V.T.T. Ha, A. Sarioglan, A. Erdem-Senatral, Y. Ben Taarit, An EPR and NMR study on Mo/HZSM-5 catalysts for the aromatization of methane: investigation of the location of the pentavalent molybdenum, *J. Mol. Catal. A Chem.* 378 (2013) 279–284, <http://dx.doi.org/10.1016/j.molcata.2013.06.020>.
- [8] X. Guo, G. Fang, G. Li, H. Ma, H. Fan, L. Yu, C. Ma, X. Wu, D. Deng, M. Wei, D. Tan, R. Si, S. Zhang, J. Li, L. Sun, Z. Tang, X. Pan, X. Bao, Direct, nonoxidative conversion of methane to ethylene, aromatics, and hydrogen, *Science* 344 (2014) 616–619, <http://dx.doi.org/10.1126/science.1253150>.
- [9] T.V. Choudhary, E. Aksyolu, D. Wayne Goodman, Nonoxidative activation of methane, *Catal. Rev.* 45 (2003) 151–203, <http://dx.doi.org/10.1081/CR-120017010>.
- [10] P. Tang, Q. Zhu, Z. Wu, D. Ma, Methane activation: the past and future, *Energy Environ. Sci.* 7 (2014) 2580–2591, <http://dx.doi.org/10.1039/C4EE00604F>.
- [11] J. Xue, Y. Chen, Y. Wei, A. Feldhoff, H. Wang, J. Caro, Gas to liquids: natural gas conversion to aromatic fuels and chemicals in a hydrogen-permeable ceramic hollow fiber membrane reactor, *ACS Catal.* 6 (2016) 2448–2451, <http://dx.doi.org/10.1021/acscatal.6b00004>.
- [12] V. Abdelsayed, D. Shekhawat, M.W. Smith, Effect of Fe and Zn promoters on Mo/HZSM-5 catalyst for methane dehydroaromatization, *Fuel* 139 (2015) 401–410, <http://dx.doi.org/10.1016/j.fuel.2014.08.064>.
- [13] J.J. Spivey, G. Hutchings, Catalytic aromatization of methane, *Chem. Soc. Rev.* 43 (2014) 792–803, <http://dx.doi.org/10.1039/c3cs60259a>.
- [14] T. Baba, H. Sawada, Conversion of methane into higher hydrocarbons in the presence of ethylene over H-ZSM-5 loaded with silver cations, *Phys. Chem. Chem. Phys.* 4 (2002) 3919–3923, <http://dx.doi.org/10.1039/b200615b>.
- [15] T. Baba, Y. Abe, Metal catalytic acidic proton bifunctional catalyst for methane activation: conversion of 13CH4 in the presence of ethylene over metal cations-loaded H-ZSM-5, *Appl. Catal. A Gen.* 250 (2003) 265–270, [http://dx.doi.org/10.1016/S0926-860X\(03\)00321-1](http://dx.doi.org/10.1016/S0926-860X(03)00321-1).
- [16] O.A. Anunziata, G.V. Gonzalez, L.B. Pierella, Catalytic activation of methane using n-pentane as co-reactant over Zn/H-ZSM-11 zeolite, *Catal. Lett.* 87 (2003) 167–171.
- [17] O.A. Anunziata, G.G. Mercado, L.B. Pierella, Improvement of methane activation using n-hexane as co-reactant over Zn/HZSM-11 zeolite, *Catal. Commun.* 5 (2004) 401–405, <http://dx.doi.org/10.1016/j.catcom.2004.04.008>.
- [18] P. He, W. Shan, Y. Xiao, H. Song, Performance of Zn/ZSM-5 for in situ catalytic upgrading of pyrolysis Bio-oil by methane, *Top. Catal.* 59 (2016) 86–93, <http://dx.doi.org/10.1007/s11244-015-0508-4>.
- [19] V.R. Choudhary, K.C. Mondal, S.A.R. Mulla, Simultaneous conversion of methane and methanol into gasoline over bifunctional Ga-, Zn-, In-, and/or Mo-modified ZSM-5 zeolites, *Angew. Chem. Int. Ed.* 117 (2005) 4455–4459, <http://dx.doi.org/10.1002/anie.200500694>.
- [20] M.V. Luzgin, V.A. Rogov, S.S. Arzumanov, A.V. Toktarev, A.G. Stepanov, V.N. Parmon, Understanding methane aromatization on a Zn-modified high-silica zeolite, *Angew. Chem. Int. Ed.* 47 (2008) 4559–4562, <http://dx.doi.org/10.1002/anie.200800317>.
- [21] A. Wang, P. He, M. Yung, H. Zeng, H. Qian, H. Song, Catalytic co-aromatization of ethanol and methane, *Appl. Catal. B Environ.* 198 (2016) 480–492, <http://dx.doi.org/10.1016/j.apcatb.2016.06.013>.
- [22] P. He, L. Zhao, H. Song, Bitumen partial upgrading over Mo/ZSM-5 under methane environment: methane participation investigation, *Appl. Catal. B Environ.* 201 (2017) 438–450, <http://dx.doi.org/10.1016/j.apcatb.2016.08.055>.
- [23] P. He, Y. Wen, J. Jarvis, R. Gatip, D. Austin, H. Song, Selective participation of methane in olefin upgrading over Pd/ZSM-5 and Ir/ZSM-5: investigation using deuterium enriched methane, *ChemistrySelect* 2 (2017) 252–256, <http://dx.doi.org/10.1002/slct.201601625>.
- [24] V.R. Choudhary, A.K. Kinage, T.V. Choudhary, Low-temperature nonoxidative activation of methane over H-galloaluminosilicate (MFI) zeolite, *Science* 275 (1997) 1286–1288, <http://dx.doi.org/10.1126/science.275.5304.1286>.
- [25] P. He, Y. Lou, H. Song, Olefin upgrading under methane environment over Ag-Ga/ZSM-5 catalyst, *Fuel* 182 (2016) 577–587, <http://dx.doi.org/10.1016/j.fuel.2016.05.126>.
- [26] P. He, R. Gatip, M. Yung, H. Zeng, H. Song, Co-aromatization of olefin and methane over Ag-Ga/ZSM-5 catalyst at low temperature, *Appl. Catal. B Environ.* 211 (2017) 275–288, <http://dx.doi.org/10.1016/j.apcatb.2017.04.052>.
- [27] J.F. Wu, S.M. Yu, W.D. Wang, Y.X. Fan, S. Bai, C.W. Zhang, Q. Gao, J. Huang, W. Wang, Mechanistic insight into the formation of acetic acid from the direct conversion of methane and carbon dioxide on zinc-modified H-ZSM-5 zeolite, *J. Am. Chem. Soc.* 135 (2013) 13567–13573, <http://dx.doi.org/10.1021/ja406978q>.
- [28] A.A. Gabrienko, S.S. Arzumanov, I.B. Moroz, A.V. Toktarev, W. Wang, A.G. Stepanov, Methane activation and transformation on Ag/H-ZSM-5 zeolite studied with solid-state NMR, *J. Phys. Chem. C* 117 (2013) 7690–7702, <http://dx.doi.org/10.1021/jp4006795>.
- [29] A. Wang, D. Austin, A. Karmakar, G.M. Bernard, V.K. Michaelis, M.M. Yung, H. Zeng, H. Song, Methane upgrading of acetic acid as a model compound for a biomass-derived liquid over a modified zeolite catalyst, *ACS Catal.* 7 (2017) 3681–3692, <http://dx.doi.org/10.1021/acscatal.7b00296>.
- [30] L. Zhang, H. Liu, X. Li, S. Xie, Y. Wang, W. Xin, S. Liu, L. Xu, Differences between ZSM-5 and ZSM-11 zeolite catalysts in 1-hexene aromatization and isomerization, *Fuel Process. Technol.* 91 (2010) 449–455, <http://dx.doi.org/10.1016/j.fuproc.2009.12.003>.
- [31] U. Olsbye, S. Svelle, M. Bjørgen, P. Beato, T.V.W. Janssens, F. Joensen, S. Bordiga, K.P. Lillerud, Conversion of methanol to hydrocarbons: how zeolite cavity and pore size controls product selectivity angewandte, *Angew. Chem. Int. Ed.* 51 (2012) 5810–5831, <http://dx.doi.org/10.1002/anie.201103657>.
- [32] Y.S. Bhat, J. Das, K.V. Rao, A.B. Halgeri, Inactivation of external surface of ZSM-5: zeolite morphology, crystal size, and catalytic activity, *J. Catal.* 159 (1996) 368–374, <http://dx.doi.org/10.1006/jcat.1996.0099>.
- [33] K. Miyake, Y. Hirota, K. Ono, Y. Uchida, S. Tanaka, N. Nishiyama, Direct and selective conversion of methanol to para-xylene over Zn ion doped ZSM-5/silicalite-1 core-shell zeolite catalyst, *J. Catal.* 342 (2016) 63–66, <http://dx.doi.org/10.1016/j.jcat.2016.07.008>.
- [34] J. Zhang, W. Qian, C. Kong, F. Wei, Increasing para-Xylene selectivity in making aromatics from methanol with a surface-modified Zn/P/ZSM-5 catalyst, *ACS Catal.* 5 (2015) 2982–2988, <http://dx.doi.org/10.1021/acscatal.5b00192>.
- [35] H. Zhang, Y. Ma, K. Song, Y. Zhang, Y. Tang, Nano-crystallite oriented self-assembled ZSM-5 zeolite and its LDPE cracking properties: effects of accessibility and strength of acid sites, *J. Catal.* 302 (2013) 115–125, <http://dx.doi.org/10.1016/j.jcat.2013.03.019>.
- [36] T.L. Cui, W.Y. Ke, W.B. Zhang, H.H. Wang, X.H. Li, J.S. Chen, Encapsulating palladium nanoparticles inside mesoporous MFI zeolite nanocrystals for shape-selective catalysis, *Angew. Chem. Int. Ed.* 55 (2016) 9178–9182, <http://dx.doi.org/10.1002/anie.201602429>.
- [37] D.B. Lukyanov, T. Vazhnova, Aromatization activity of gallium containing MFI and TON zeolite catalysts in n-butane conversion: effects of gallium and reaction conditions, *Appl. Catal. A Gen.* 316 (2007) 61–67, <http://dx.doi.org/10.1016/j.apcata.2006.09.019>.
- [38] F. Marques Mota, P. Eliášová, J. Jung, R. Ryoo, Impact of pore topology and crystal thickness of nanoporous zeolites on the hydroconversion of ethylbenzene, *Catal. Sci. Technol.* 6 (2016) 2653–2662, <http://dx.doi.org/10.1039/C5CY02029H>.
- [39] S. Teketel, U. Olsbye, K. Lillerud, P. Beato, S. Svelle, Microporous and mesoporous materials selectivity control through fundamental mechanistic insight in the conversion of methanol to hydrocarbons over zeolites, *Microporous Mesoporous Mater.* 136 (2010) 33–41, <http://dx.doi.org/10.1016/j.micromeso.2010.07.013>.
- [40] X. Li, Q. Sun, Y. Li, N. Wang, J. Lu, J. Yu, Confinement effect of zeolite cavities on methanol-to-olefin conversion: a density functional theory study, *J. Phys. Chem. C* 118 (2014) 24935–24940, <http://dx.doi.org/10.1021/jp505696m>.
- [41] M.E. Martínez-Armero, M. Moliner, G. Sastre, F. Rey, C. Martínez, A. Corma, ITQ-39 zeolite, an efficient catalyst for the conversion of low value naphtha fractions into diesel fuel: the role of pore size on molecular diffusion and reactivity, *J. Catal.* 333 (2016) 127–138, <http://dx.doi.org/10.1016/j.jcat.2015.10.024>.
- [42] N. Kosinov, F.J.A.G. Coumans, E.A. Uslamian, A.S.G. Wijpkema, B. Mezari, E.J.M. Hensen, Methane dehydroaromatization by Mo/HZSM-5: mono- or bifunctional catalysis? *ACS Catal.* 7 (2017) 520–529, <http://dx.doi.org/10.1021/acscatal.6b02497>.
- [43] W. Ding, G.D. Meitzner, E. Iglesia, The effects of silanation of external acid sites on the structure and catalytic behavior of Mo/H-ZSM5, *J. Catal.* 206 (2002) 14–22, <http://dx.doi.org/10.1006/jcat.2001.3457>.
- [44] K.R. Kahsar, D.K. Schwartz, J.W. Medlin, Control of metal catalyst selectivity through specific noncovalent molecular interactions, *J. Am. Chem. Soc.* 136 (2014) 520–526, <http://dx.doi.org/10.1021/ja411973p>.
- [45] H.J. Davis, R.J. Phipps, Harnessing non-covalent interactions to exert control over regioselectivity and site-selectivity in catalytic reactions, *Chem. Sci.* 107 (2017) 5713–5743, <http://dx.doi.org/10.1039/C6SC04157D>.
- [46] K. Kim, T. Lee, Y. Kwon, Y. Seo, J. Song, J.K. Park, H. Lee, J.Y. Park, H. Ihee,

- S.J. Cho, R. Ryoo, Lanthanum-catalysed synthesis of microporous 3D graphene-like carbons in a zeolite template, *Nature* 535 (2016) 131–135, <http://dx.doi.org/10.1038/nature18284>.
- [47] H. Tao, H. Yang, X. Liu, J. Ren, Y. Wang, G. Lu, Highly stable hierarchical ZSM-5 zeolite with intra- and inter-crystalline porous structures, *Chem. Eng. J.* 225 (2013) 686–694, <http://dx.doi.org/10.1016/j.cej.2013.03.109>.
- [48] C. Fernandez, I. Stan, J.P. Gilson, K. Thomas, A. Vicente, A. Bonilla, J. Pérez-Ramírez, Hierarchical ZSM-5 zeolites in shape-selective xylene isomerization: role of mesoporosity and acid site speciation, *Chem. A Eur. J.* 16 (2010) 6224–6233, <http://dx.doi.org/10.1002/chem.200903426>.
- [49] K. Lee, M. Choi, Hierarchically micro-/mesoporous Pt/KL for alkane aromatization: synergistic combination of high catalytic activity and suppressed hydrogenolysis, *J. Catal.* 340 (2016) 66–75, <http://dx.doi.org/10.1016/j.jcat.2016.05.010>.
- [50] J. Pérez-Ramírez, C.H. Christensen, K. Egeblad, C.H. Christensen, J.C. Groen, Hierarchical zeolites: enhanced utilisation of microporous crystals in catalysis by advances in materials design, *Chem. Soc. Rev.* 37 (2008) 2530–2542, <http://dx.doi.org/10.1039/b809030k>.
- [51] H. Zhang, Z. Hu, L. Huang, H. Zhang, K. Song, L. Wang, Z. Shi, J. Ma, Y. Zhuang, W. Shen, Y. Zhang, H. Xu, Y. Tang, Dehydration of glycerol to acrolein over hierarchical ZSM-5 zeolites: effects of mesoporosity and acidity, *ACS Catal.* 5 (2015) 2548–2558, <http://dx.doi.org/10.1021/cs5019953>.
- [52] H. Chen, Y. Wang, F. Meng, H. Li, S. Wang, C. Sun, S. Wang, X. Wang, Conversion of methanol to propylene over nano-sized ZSM-5 zeolite aggregates synthesized by a modified seed-induced method with CTAB, *RSC Adv.* 6 (2016) 76642–76651, <http://dx.doi.org/10.1039/C6RA14753D>.
- [53] J.C. Groen, J.A. Moulijn, J. Pérez-Ramírez, Decoupling mesoporosity formation and acidity modification in ZSM-5 zeolites by sequential desilication-dealumination, *Microporous Mesoporous Mater.* 87 (2005) 153–161, <http://dx.doi.org/10.1016/j.micromeso.2005.07.050>.
- [54] Z. Wang, J. Wang, T.K. Sham, S. Yang, Tracking the interface of an individual ZnS/ZnO nano-heterostructure, *J. Phys. Chem. C.* 116 (2012) 10375–10381, <http://dx.doi.org/10.1021/jp301289x>.
- [55] S. Kotrel, H. Knözinger, B.C. Gates, The Haag-Dessau mechanism of protolytic cracking of alkanes, *Microporous Mesoporous Mater.* 35–36 (2000) 11–20, [http://dx.doi.org/10.1016/S1387-1811\(99\)00204-8](http://dx.doi.org/10.1016/S1387-1811(99)00204-8).
- [56] A. Bhan, W. Nicholas Delgass, Propane aromatization over HZSM-5 and Ga/HZSM-5 catalysts, *Catal. Rev.* 50 (2008) 19–151, <http://dx.doi.org/10.1080/01614940701804745>.
- [57] H.J. Park, H.S. Heo, J.K. Jeon, J. Kim, R. Ryoo, K.E. Jeong, Y.K. Park, Highly valuable chemicals production from catalytic upgrading of radiata pine sawdust-derived pyrolytic vapors over mesoporous MFI zeolites, *Appl. Catal. B Environ.* 95 (2010) 365–373, <http://dx.doi.org/10.1016/j.apcata.2010.01.015>.
- [58] E. Pretsch, P. Buhlmann, M. Badertscher, *Structure Determination of Organic Compounds*, Springer, Berlin Heidelberg, 2009, <http://dx.doi.org/10.1007/978-3-540-93810-1>.
- [59] L. Remusat, P. Hatton, P.S. Nico, B. Zeller, M. Kleber, D. Derrien, NanoSIMS study of organic matter associated with soil aggregates: advantages, limitations, and combination with STXM, *Environ. Sci. Tech.* 46 (2012) 3943–3949, <http://dx.doi.org/10.1021/es203745k>.